LOSS OF SKELETAL MUSCLE PKCθ PROTECTS AGAINST THE PATHOGENESIS OF INSULIN RESISTANCE

by

Bailey Dakota Peck

A thesis submitted to the faculty of
The University of North Carolina at Charlotte
in partial fulfillment of the requirements
for the degree of Master of Science in
Kinesiology

Charlotte

2016

Approved by:

_____
Dr. Joseph Marino

_____
Dr. Susan Arthur

_____
Dr. Jeanette Bennett

_____
Dr. Terry Hinds Jr.

ABSTRACT

BAILEY DAKOTA PECK. Loss of skeletal muscle PKCθ protects against the pathogenesis of insulin resistance. (Under the direction of DR. JOSEPH MARINO)

Skeletal muscle is a primary regulator of glucose homeostasis, accounting for the majority of post-prandial glucose disposal. However states of skeletal muscle insulin-resistance result in severely attenuated glucose uptake and consequently hyperglycemia. The underlying cause of insulin-resistance in obese populations is currently theorized to be the consequence of lipotoxicity, but as of yet the intramyocellular mechanisms for this response remain elusive. Lipid intermediates such as diacylglycerol possess a high affinity for ligand binding/activation of protein kinase C (PKC) isoforms. PKC isoform θ specifically, has a strong correlation with lipid accumulation and insulin-stimulated glucose uptake inhibition. In order to investigate PKCθ's role in skeletal muscle insulin-resistance, a muscle specific PKCθ knock out mouse model was employed followed by a 15 week high fat diet. The phenotype exhibited by our skeletal muscle PKCθ knock out mice is one of reduced weight gain, lipid accumulation, inflammation, and insulin resistance compared to wild type controls. The immunity to such deleterious effects regularly witnessed in high fat fed wild type mice further illustrates the prominent manner by which PKCθ induces skeletal muscle insulin-resistance.

TABLE OF CONTENTS

INTRODUCTION

Skeletal muscle is a primary regulator of glucose homeostasis, accounting for the majority of post-prandial glucose disposal. Dysfunction in skeletal muscle insulin and glucose metabolism, as observed with diet/inactivity-induced obesity, is an established cause of hyperglycemia. Importantly, hyperglycemia is a predictor of type 2 diabetes (T2D) and based on current trends, 438 million people worldwide will have T2D by year 2030 (International Diabetes Federation). A deeper understanding of how high fat diets contribute to skeletal muscle insulin and glucose intolerance may highlight novel pharmacological pathways to slow the progression of T2D and supplement appropriate lifestyle modifications.

The mechanisms underlying insulin-resistance (IR) in obese populations may be of genetic, environmental, or lifestyle origin, or a combination of these factors, indicating that interventions may require a multifactorial approach [1]. One theory behind obesity-related skeletal muscle IR is centered on lipotoxicity; an accumulation of lipid in skeletal muscle. Such a state results in the accumulation of fatty acid intermediates, such as diacylglycerol (DAG) from the incomplete oxidation of fatty acids. When not completely metabolized, DAG can signal through a second messenger system, causing skeletal muscle IR. The detrimental effects of skeletal muscle IR may contribute to dysfunction of other tissues, including the liver and pancreas [2].

The molecular basis for obesity-induced IR is complex; however serine/threonine kinase's that target the insulin receptor and its downstream substrates/targets have been identified as major contributors [3, 4]. One serine/threonine kinase in particular has received considerable attention for its involvement in the pathogenesis of insulin

resistance, protein kinase C (PKC) θ [5]. Although PKCθ transcripts are ubiquitously expressed, the highest levels are found in hematopoietic and skeletal muscle cells [6, 7]. The specificity for DAG/phorbol-ester binding implicates PKCθ as a potential therapeutic target in mitigating free fatty acid (FFA) induced insulin resistance [8].

Early clinical studies in humans, demonstrated an elevated expression of PKCθ in patients with T2D, which inversely correlated with insulin sensitivity [9]. In a study designed to understand the mechanisms underlying lipid induced IR in human skeletal muscle, muscle biopsies from lean, healthy subjects were analyzed during a lipid infusion as well as muscle biopsies from T2D subjects [10]. The findings revealed that the accumulation of membrane localized DAG resulted in PKCθ activation at the onset of IR in healthy subjects, with no accompanying alterations in muscle ceramide, acylcarnitine content or adipocytokines [10]. Comparable outcomes were also present in the muscle biopsies of T2D subjects. Lipid infusion is an effective acute model of FFA induced IR. However, obesity and T2D are not a consequence of an acute exposure to elevated lipids but rather a product of chronically elevated levels that result in multi-tissue IR. In order to examine the importance of skeletal muscle PKCθ in IR/obesity/T2D, long term studies using high fat feeding are needed to assess the underlying mechanisms that link PKCθ and skeletal muscle IR.

Under sedentary conditions, skeletal muscle is particularly reliant upon insulin signaling to stimulate glucose uptake and manage glycemic status [11]. Acute IR can attenuate this process, causing hyperglycemia, resulting in a hyperinsulinemic response [2]. The burden of sustaining this insulin response to offset hyperglycemia in IR subjects contributes to β-cell exhaustion [2]. The onset of IR in obese populations currently lacks

a definitive point of origin, leaving many to speculate as to which obesity driven symptom (hyperlipidemia, hyperglycemia, hyperinsulinemia, hypercortisolism and inflammation) acts as the stimulus and which is merely a symptom of the other. The consequence of which, forces many investigators to focus on one or two areas they feel could benefit the field of IR the greatest. Regrettably this has failed to produce much of an impact on a growing patient population. With the understanding that skeletal muscle behaves as a secretory organ, it is vital to understand its systemic effects when insulin sensitivity is maintained despite an environment that promotes a state of IR.

The overall objective of this study was to investigate the contribution of skeletal muscle PKCθ expression in the pathogenesis of diet-induced obesity and insulin resistance. To do so our group utilized the Cre-Lox transgenic approach to bread mice that lack PKCθ specifically in skeletal muscle ($SkM^{PKC\theta KO}$), avoiding any confounding variables (e.g., adipose, liver, cardiac and immune function) that may have arisen from other universal knockout models. Following 15 weeks on a high fat diet (HFD), $SkM^{PKC\theta KO}$ mice had abrogated weight gain, lower fasting glucose, maintained insulin sensitivity, and had low skeletal muscle lipid accumulation. Taken together, our study demonstrates that skeletal muscle PKCθ is a major contributor to the events that perturb insulin and glucose homeostasis. These findings further our understanding of the pathogenesis of skeletal muscle insulin resistance, identifying PKCθ as a potential therapeutic target for IR and simultaneously linking PKCθ as a prominent conduit for FFA induced IR.

LITERATURE REVIEW

Protein kinase C (PKC) isoforms are classified among three groups with discrepancies in the N-terminal regulatory co-factor-binding domain; 1) Novel (δ, ε, θ, and η), which are regulated by DAG or phorbol ester regulation 2) Conventional (α, βI, βII and γ), which are regulated by Ca^{2+}, DAG, or phorbol ester interactions, and 3) Atypical (ι, ζ, λ, and μ), which are regulated solely by protein-protein interaction [12]. PKCθ is a DAG sensitive 706 amino acid long single polypeptide, with a high affinity for serine or threonine residue phosphorylation [13]. Structural similarities are shared between PKCθ and other members of the PKC family, which include a regulatory N-Terminal domain and a C-terminal catalytic domain joined by a hinge region [13].

PKCθ, like its fellow novel members, has a regulatory domain which consists of a CIa and CIb domain that have DAG and phorbol ester binding sites and a C2 domain variant incapable of binding Ca^{2+} [13]. A pseudosubstrate within CIa inhibits enzymatic activity in the absence of DAG or phorbol esters. The binding of DAG to CIb domain effectively releases the inhibitory pseudosubstrate and enhances PKCθ's interaction with acidic phosphatidylserine [12]. DAG binding causes PKCθ to relocate from the sarcoplasm to the sarcolemma. Markers for PKCθ activation outside of its cellular translocation include serine/threonine phosphorylation. Threonine 538 (Thr538) phosphorylation, a key residue in the autophosphorylation loop, is used as a surrogate for activation of PKCθ [14]. Research supporting this claim reported a 570% increase in PKCθ Thr538 phosphorylation compared to controls, following the treatment of C_2C_{12} cells with palmitate [15]. Of the 12 PKC isoforms, 4 have been implicated in IR [16].

Not surprising, 3 are from the novel PKC subclass (ε, δ, and θ), with PKCε receiving considerable attention for its phosphoinositide-dependent kinase (PDK-1) directed nuclear transrepressive activity of insulin receptor expression [17]. Similar transgenic KO models have been applied when attempting to understand the role of PKCδ in IR. Although muscle-specific deletion did not rescue young mice from the effects of a HFD, $SkM^{PKC\delta KO}$ mice as they aged (15-month old), exhibited lower metabolic rates and reduced mitochondrial mass [18].

Obesity is now endemic, and one of the strongest predictors for T2D [19]. Current estimates suggest that 1 in 3 Americans will be effected by this disease within the next 40 years [20]. Weight loss through diet and exercise has consistently been used to demonstrate the reversal of IR in obese subjects [19]. The mechanisms by which this is enacted are only partially understood. The extent to which diet/exercise produce said effects are the result of decreased lipid content and increased insulin-independent glucose uptake via exercise-stimulated AMPK/calmodulin kinase II (CamKII) responses, which attenuate the hyperlipidemia/hyperglycemia experienced by subjects experiencing IR when exercise is performed routinely [19, 21, 22]. Although it is well understood that IR in obese/T2D subjects can be reversed if obese individuals are able to adhere to 60-90mins of exercise a day, compliance rates among obese adults is below 3% [23]. Therefore, we still have a problem requiring a multifactorial approach to sustain positive affects in the absence of regular exercise. Therapeutic intervention's designed to mitigate IR under HFD and obesity could delay associated disease and health care cost and concomitantly enhance the effects of diet and exercise on weight loss.

Under normal homeostatic conditions insulin promotes the uptake of glucose at key storage sites e.g., liver, adipose tissue, and skeletal muscle [19], at which point glucose can either be converted to glycogen or lipids [22]. Insulin also acts to suppress lipolysis, preventing the formation of lipid intermediates that serve as second messenger hormones in inhibitory signaling pathways [24]. Lipid accumulation in adipose tissue is an important evolutionary proponent, providing efficient conversion and utilization during feeding and fasted states. Maintaining insulin sensitivity in adipose tissue enhances lipogenesis and decreases plasma FFA concentration and subsequently ectopic lipid accumulation in skeletal muscle [22].

A unique sub-population that displays a phenotype of enhanced intramyocellular lipid (IMCL) content with normal insulin sensitivity exists in most elite endurance athletes. These highly trained endurance trained athletes exhibit elevated lipid droplet size and number due to the physiological training adaptation required for extended exercise bouts [25, 26]. Enlarged adipose tissue is the product of enhanced β-oxidation, FFA uptake and storage. Ultimately resulting in metabolic defects also known as lipodystrophy [27]. In the wake of such an occurrence, macrophages infiltrate and secrete lipolytic inducing cytokines that release fatty acids into circulation, which act to flood highly metabolic tissues like skeletal muscle and the liver [27]. Based on the very relevant and daily happening of said events we feel that it is absolutely imperative to identify key lipid intermediate targets implicated in skeletal muscle IR followed swiftly by an efficacious treatment for those suffering. Excess nutrient intake, especially those dense in high fat have a taxing effect adipose tissue, the outcome of which is called lipodystrophy or adipocyte metabolism dysfunction. The mechanism by which PKCθ

inhibits intracellular insulin signaling cascades has yet to be fully uncovered, however prior research has identified key protein intermediates both in vitro and in vivo that are encroached upon by PKCθ.

In the wake of preliminary attempts to fully elucidate the underlying mechanisms behind PKCθ and its role in insulin resistance, conflicting reports surfaced arguing the importance of PKCθ in maintaining insulin sensitivity [28, 29]. The discrepancies between labs are likely a consequence of the variable PKCθ genetic deletion/inhibition models utilized, as well as the duration of treatment and study [28-31]. It is not surprising that following the initial reports stipulating PKCθ in IR, investigators set out to identify the mechanism(s) involved. However, the reports that ensued were not only contradictory to preliminary findings; they also goaded biased analysis of previous work concerning PKCθ content and localization in skeletal muscle of obese/T2D humans and rats [29].

One such study using a cardiac/skeletal muscle specific dominant negative (DN) kinase dead mutant of PKCθ in mice, reported increased adipose accumulation in mice after 6 months of age, with IR observed prior (4 months of age) [28]. Perplexingly, in vitro studies overexpressing DN-PKCθ reported opposing findings with insulin sensitivity (reduced serine1101 phosphorylation) [32]. Another caveat that was not discussed in the original DN-PKCθ work was the use of a desmin-promoter to induce the overexpression of the kinase dead PKCθ mutant isoform and its subsequent expression in cardiac tissue, which may have led to complications with insulin signaling in the heart and overall function, possibly leading to decreased activity [28]. In a similar study aimed at investigating the effects of PKCθ in obesity and IR with a high fat diet, the use of a

universal PKCθ–KO ($PKC\theta^{-/-}$) mouse model recounted identical findings to the ones seen using DN-PKCθ, with regard to increased adiposity and IR [29]. The outcomes from these studies should raise flags to those interpreting the data presented therein. Most notably the role by which PKCθ acts to inhibit insulin signaling in skeletal muscle, may also act to prevent insulin-induced lipogenesis in adipose tissue.

Extracellular receptor ligand binding is the predominant form of glucose uptake under sedentary conditions in skeletal muscle. Circulating insulin and insulin-like growth factor-1 (IGF-1) converge on extracellular insulin receptors and hybrid insulin receptor/IGF-1 receptors to initiate subcellular dimerization and activation [33]. Autophosphorylation of the activation loop in the insulin receptor tyrosine kinase domain increases its catalytic efficiency and additional tyrosine sites are then autophosphorylated, i.e., insulin receptor substrates (IRS) in proximity/contact to the activated tyrosine kinase domain [33].

IRS-1 contains multiple inhibitory serine residues that have been suggested to be either directly or indirectly targeted by PKCθ [32]. DAG activated PKCθ induces its subcellular relocation to the sarcolemma. PKCθ's redistribution is then primed for IRS-1 serine1101 phosphorylation [32]. Serine phosphorylation of residue 307 (Ser307) in 3T3-L1 adipocytes occurs via PKCθ downstream proponents; inhibitor κB kinase-β (IKK-β) and c-JUN NH_2-terminal kinase (JNK) [4]. Though no study has yet to illustrate this indirect mechanism in vivo, it would not be a stretch to conclude that FFA induced phosphorylation of Ser307 via IKK-β is mediated in some form or fashion by PKCθ [34]. In lieu of recent accusations that increased IRS-1 serine phosphorylation and/or decreased IRS-1 protein content are not acutely associated with IR in skeletal muscle, one

must take in account that these manipulations were limited to the tibialis cranialis (TC) and the data presented while not significant, appeared to be trending towards a reduction in glucose uptake in the short hairpin (sh) RNA-mediated IRS-1 TC limb versus control TC limb [35]. Lipid and insulin infusion-induced skeletal muscle resistance has also received considerable scrutiny. At the molecular level, a number of studies have linked dysfunctional glucose metabolism with alterations in pyruvate dehydrogenase kinase (PDK4) content and pyruvate dehydrogenase complex (PDHC) activity, without the expected decrease of IRS-1 tyrosine phosphorylation [36]. In the case of PKCθ, those who failed to reproduce this in HFD reasoned that the difference between acute and chronic lipid treatment is that tissue with higher insulin sensitivity, will also have greater lipid uptake and lower infusion rate prior to the onset of IR [29]. Respectfully, this argument was later disproved using a PKCθ pseudosubstrate in C_2C_{12}'s to reduce serine phosphorylation of IRS-1 by mammalian target of rapamycin (mTOR) and ribosomal protein S6 kinase (S6K) following palmitate treatment [37]. Prior to this finding, increased serine phosphorylation of IRS-1 was highly implicated in the disconnect between insulin secretion and glucose uptake in skeletal muscle [38].

Inhibition of IRS-1 activity is associated with reduced recruitment and binding to the Src homology 2 (SH2)-domain of the p85 regulatory subunit of class IA phosphatidylinositol 3-kinase (PI3K) [3, 39]. PI3K exists as a heterodimer, which consists of the p110 (α/β) catalytic subunit in addition to its p85 regulatory subunit. PI3K's interaction with IRS-1 is a necessary step for catalytic addition of a phosphate group to the 3'-position of the inositol ring of the membrane lipid phosphatidylinositol (PtdIns) [39]. The synthesis of intracellular PtdIns (3,4,5)-triphosphate (PIP_3) from

PtdIns(4,5)P_2 in response to insulin induces a rapid 500-fold increase in PIP_3 over baseline [40]. PIP_3 interaction is an indispensable proponent to a variety of cell functions (cell progression, cell survival, apoptosis, cellular growth, cytoskeletal rearrangement and intracellular vesicle tracking) [39]. The pleckstrin homology domain of the effector proteins permits the inositol head group of PIP_3 to bind and produce a conformational change that stimulates the dissemination of downstream signaling cascades relevant to the previously mentioned cell functions [40].

One of the most prominent downstream kinases in insulin signaling that is known to interact with PIP_3 is Akt (also known as protein kinase B) and among the 3 Akt family species (Akt1 to -3), Akt2 displays the greatest effect on glucose metabolism [41, 42]. The interaction between PIP_3 and Akt allows two other kinases; 3-phosphoinositide-dependent protein kinase 1 (PDK1) and mTOR complex 2 (mTORC2) to phosphorylate and activate Akt [43]. Akt possess two key phosphorylation sites (Ser473 and Thr308), both of which are required to produce Akt's phospho-regulation of glucose uptake [42]. Interestingly, stimulating PKCθ serine/threonine kinase activity with phorbol 12-myristate 13-acetate (PMA) effectively reduced phosphorylation of both Akt phosphorylation sites via two similar yet distinct mechanisms [44]. Decreased Ser473 phosphorylation is the product of PKCθ's inhibitory serine phosphorylation of IRS-1and reducing its affinity for PI3K, which effectively attenuates PIP_3 accumulation, such that PIP_3 can no longer position Akt for mTORC2 phosphorylation [32]. In addition to reducing Akt's translocation to the plasma membrane, mTORC2 activation also occurs via PIP_3's PH-domain binding with stress-activated map kinase-interacting protein 1 (SIN1) [45]. Following PIP_3 and SIN1 binding, mTORC2 is effectively released

triggering phosphorylation of Ser473 [45]. In a more direct fashion, PKCθ has been shown to mediate the inhibition of PDK1 via Ser504 and Ser532 [31]. This was followed by stark decrease in the phosphorylation of Thr308 on Akt (1/2) [31]. In T2D subjects, the attenuation of Akt and impaired glucose uptake is associated aberrant Akt substrate of 160 kDa (AS160) phosphorylation [44]. This defect prohibits the release and translocation of the glucose transporter type 4 to the cell membrane, where it facilitates the diffusion of circulating glucose into the cell [44]. This intracellular defect ultimately results in one the primary consequences of IR, an inability to maintain normal homeostatic blood glucose levels.

The overall objective of this study was to expand on the primary mechanisms observed in vitro that have implicated PKCθ in skeletal muscle IR, and begin to reconcile the inconsistencies among in vivo models. Through the use of a proven in vivo knockout approach (Cre/lox), we will ascertain the true nature in which PKCθ participates in skeletal muscle insulin signaling. The data presented here also contributes our understanding of how dysfunction in skeletal muscle contributes to changes in other physiological systems when challenged by a HFD. To test the hypothesis that $SkM^{PKC\theta KO}$ prevents diet induced IR we subjected male mice to 15-wk of a regular diet (RD) or HFD. Our data revealed that $SkM^{PKC\theta KO}$ mice not only maintained insulin sensitive equal to RD mice but also displayed a significant attenuation in weight gain and improvements in other variables associated with IR, compared to HFD-fed $SkM^{PKC\theta WT}$ mice.

METHODS

Generation of $SkM^{PKC\theta KO}$ Mice. The UNC Charlotte Institutional Animal Care and Use Committee approved all laboratory animal procedures. Protocol ID: 13-007 and 14-010. 33 male mice of mixed 129/C57/FVB background were used in this study. All of the mice were housed in the vivarium facility at the University of North Carolina at Charlotte with a 12: 12-h light-dark cycle and constant temperature (22-25^{0}C), with free access to water and diet. In order to generate $SkM^{PKC\theta KO}$ offspring, C57/FVB males heterozygous for a modified Cre-recombinase (iCre) designed to replace exon 1 of the myogenic differentiation 1 (Myod1) gene were paired with 129/C57 females homozygous for the PKCθ loxP-flanked (floxed) allele [46]. Male offspring homozygous for the PKCθ floxed allele and heterozygous for the Myod1-iCre allele were then split into regular chow diet (RD) or HFD (60% Fat) groups at weaning (3-wk). PKCθ floxed allele littermates absent for Myod1-iCre were used as controls and split into either RD or HFD cohorts. The sample size for each group was: n = 6 RD-$SkM^{PKC\theta WT}$, n = 7 HFD-$SkM^{PKC\theta WT}$, n = 10 RD-$SkM^{PKC\theta KO}$ and n = 10 HFD-$SkM^{PKC\theta KO}$. The 4 groups where then subjected to 15-wk of their respective diet, with mouse weights taken weekly. At 18-wk of age following an overnight (16-h) fast, mice were given an IP of insulin (Humulin R U-100) at a desired dose of 10-UI/kg of body weight. After 15-min, mice were placed under anesthesia (Isoflurane) and tissue was collected from the hind limbs (Gastrocnemius, Plantaris and Soleus) as well as the heart, liver, adipose tissue and blood. Animals were subject to cervical dislocation prior to cardiac puncture. Tissue was weighed and then snap-frozen in isopentane or liquid nitrogen and stored at -80^{0}C until processing.

Genotyping. Mice were routinely genotyped by PCR using DNA extracts from tail clips at 2-wk of age. Tail clips were washed once in 70% ethanol and placed in ice prior to DNA extraction using RedExtract-N-AMP tissue PCR kit (Sigma-Aldrich). Primers directed towards intron 4 of PKCθ (fwd-TACATCCAGAAAAAGCCAACCA, rev-TTCTGTCCGCCCATTGTTCT) (Eurofin) were used to detect the band WT band (425bp) and floxed allele (459bp). PCR was performed using a cocktail of 4µl of genomic DNA, 0.2µl fwd/rev primers, and 10µl RedExtract Master Mix (MM) solution in the Mastercycler Gradient PCR machine (Eppendorf) under the following conditions; 1 cycle (95°C x 3-min), 35 cycles (94° x 30-s, 64° x 30-s, 72° x 1-min), end cycle (72° x 10-min). Amplified DNA was then analyzed using southern blot with a 2% agarose (Fisher Scientific) gel in Tris-acetate-EDTA buffer (VWR). Bands were identified using ethidium bromide (ThermoFisher) under UV light (365nm) on the Benchtop 2UV Transilluminator (UVP). PKCθ floxed mouse DNA extracts were used under similar conditions for MyoD-iCre identification with primers directed toward the mutant iCre (149bp) allele (fwd-CGGCTACCCAAGGTGGAGAT, rev-TGGGTCTCCAAAGCGACTCC).

Glucose Tolerance Testing. At 15-wk of age, mice were given an intraperitoneal glucose tolerance test (IPGTT) following a 6-h fast. Glucose was taken just prior to dextrose injection (1mg/g body weight) and then 15, 30, 45, 60, 90, and 120 minutes post injection blood from the tail vein using laboratory animal-specific hand held glucometer and test strips (Alpha Trak).

Western Blot Analysis. Frozen Tissue samples (gastrocnemius, soleus, plantaris, and adipose tissue) were homogenized as previously described [47]. Tissue samples were homogenized in ice-cold RIPA Buffer (ThermoFisher) containing 1xprotease/phosphatase inhibitor cocktails (Pierce) via bead milling (Benchmark Beadblaster24). Lysates were then gently rocked end-over-end for 30 mins at 4°C followed by centrifugation for 30-min at 16,000xg to pellet any debris. Pre-cleared lysates were then analyzed for protein content using BCA protein assay (ThermoFisher).

SDS-PAGE was performed using Nusep Tris-glycine precast gels. 30-50μgs of protein were loaded with 4xloading buffer (Licor) and 400mM Dithiothreitol (Invitrogen) Proteins were separated at 200V for 50 mins at 4°C. 0.45μm pore size polyvinylidene fluoride (PVDF) membranes (Millipore) were activated using 100% methanol (Fisher Scientific) followed by a 2-min wash in deionized H_2O. Electroblotting was carried out under constant volts (100V) for 2.5-hr in Tris-glycine transfer buffer (Fisher Scientific) supplemented with 10% methanol. Upon completion membranes were washed twice in Tris buffered saline (TBS) and blocked for 1-hr in Odyssey blocking buffer (Licor) at room temperature (RT). Blocking buffer was removed and membranes were washed twice in TBS-0.1% tween (TBST) and incubated overnight (16-hr) at 4°C with primary antibodies (Cell Signaling Technologies), diluted in 5% bovine serum albumin (BSA)-TBST (Sigma-Aldrich) at a concentration of 1:1000. The list of antibodies used were as follows; rabbit anti-mouse Akt Ser473, rabbit anti-mouse Akt Thr308, mouse anti-mouse Akt total, rabbit anti mouse IRS-1 total, rabbit anti mouse PKCθ total, rabbit anti mouse FABP4, mouse anti mouse GAPDH (Millipore) and mouse anti mouse β-actin (Sigma-Aldrich). Following the removal of primary antibodies, membranes were washed three

times in TBST and secondary antibodies (Licor) diluted in 5% BSA-TBST at a concentration of 1:10000 were added (donkey anti rabbit IRDye 680RD and goat anti mouse IRDye 800CW) for 2 hours at room temperature (RT). Prior to imaging, membranes were washed 3 times in TBST followed by 2 more washes in TBS to remove residual tween. Fluorescent imaging was carried out using the Odyssey imaging system (Licor) and analysis of bands was performed using Odyssey software (Licor). Proteins probed for phosphorylation were normalized to respective total protein expression. Other proteins were normalized to beta actin or GAPDH.

Immunoprecipitation of IRS-1 Protein. Immunoprecipitation (IP) IRS-1 was performed using Dynabeads protein A IP kit. 500μg of protein were incubated with 5μg of rabbit anti mouse IRS-1 antibody overnight at 4°C with gentle end-over-end rotation. Antigen-antibody complexes were then transferred to an Eppendorf tube containing 100μl of protein A Dynabeads. Antigen-antibody-bead solutions were placed at 4°C for 8 hours with gentle end-over-end rotation, followed by magnetic separation to remove the unbound protein lysate. Non-specific binding was removed with three washes in phosphate buffered saline-0.1% tween (PBST) washes followed by bead-antibody-antigen dissociation with 40μl elution buffer for 2-min and then neutralized with 1M Tris, pH 7.5. Eluted samples were then subjected to western blot for further analysis. Cell Signaling Technologies primary antibodies; rabbit anti mouse IRS-1 Ser1101 and mouse anti mouse IRS-1 total were used following western blot.

RNA Isolation and RT PCR. Prior to freezing tissue samples at -80°C, skeletal muscle being stored for RNA extraction were placed in RNALater (Qiagen) for 24-hr at 4°C. The tissues were removed from RNALater and stored at -80°C. Prior to homogenization, tissues were weighed and minced according to manufacturer's instructions (Qiagen). RNA homogenization buffer was supplemented with 10mM beta mercaptoethanol (Fisher Scientific) and tissue samples were homogenized at RT in Beadblaster24. Spin column purification using RNA fibrous tissue mini kit (Qiagen) was performed and eluted with 40µl RNase free-H_2O. Eluted RNA quality was measured with NanoDrop 1000 spectrophotometer (ThermoFisher) and only high quality RNA (260/280 reading between 1.8-2.1) samples were converted to cDNA using Applied Biosystems cDNA synthesis kit (1µg of RNA/reaction). Samples containing cDNA were diluted to 5ng/µl in 18-MΩ H_2O. Real time PCR was performed on a Step One Plus system (Applied Biosystems) using SYBR green/high ROX reagent (ASI). Fold change in expression levels was determined using $2^{-\Delta\Delta CT}$ with GAPDH as control gene. Real-time PCR primer sequences are listed in Table 1.

Table 1: Primer sequences

	Sequence 5' to 3'
GAPDH	Forward: ATGTTTGTGATGGGTGTGAA Reverse: ATGCCAAAGTTGTCATGGAT
PKCθ	Forward: TACATCCAGAAAAAGCCAACCA Reverse: TTCTGTCCGCCCATTGTTCT
PKCδ	Forward: GCCAGAAGTCTCTGGGAGTG Reverse: AAAGCTGCCTTTGCCAAGTA
PKCε	Forward: GATCGAGCTGGCTGTCTTTC Reverse: TCCAGGTCAATCCAGTCCTC
PKCη	Forward: AAAGTGGATGCCAAGATTGC Reverse: CGTTGAACTTGTGTGGGATG
PKCα	Forward: GTTTACCCGGCCAACGACT Reverse: TCATGCACGTTCTTCTGCCT
MuRF1	Forward: GGGGGTCAGGGGACGAAGACA Reverse: TCTCGCCCACCTGCGTCACA
MAFbx	Forward: CCAGGATCCGCAGCCCTCCA Reverse: ATGCGGCGCGTTGGGAAGAT
TNF-α	Forward: CCAGACCCTCACACTCAGATC Reverse: CACTTGGTGGTTTGCTACGAC
PGC-1α	Forward: TGATGTGAATGACTTGGATACAGACA Reverse: GCTCATTGTTGTACTGGTTGGATATG

Oil Red O Staining and Analysis of IMCL Content. Tissues snap frozen in liquid nitrogen chilled isopentane were used for all histochemical analysis. The gastrocnemius was cut in 10μm thick sections using a cryostat (Microm) and mounted on charged microscope slides (ASI) and stored at -20°C until further processing. Oil Red O staining was performed as previously described [48]. Slides were removed from -20°C freezer and allowed to thaw at RT for 5-min. Following fixation in 4% paraformaldehyde (PFA) in PBS, pH 7.4, slides were washed with deionized H_2O (3x30-sec). Oil red o stock solution was prepared using 500mg oil red o (Sigma-Aldrich) in 100ml 60% Triethyl-phosphate (Sigma-Aldrich) and deionized H_2O. Working solution was prepared using 12ml oil red o stock solution and 8ml deionized water. Working solution was then filtered through a 0.45μm filter (ASI) and placed in a light protected complin Jar with

slides for 30-min at RT. The slides were then washed in deionized H_2O (3x30-sec) and then rinsed under running tap water for 10-min. Slides were mounted with 10% glycerol in PBS and cover slipped. Mounted slides were imaged using IX71 Microscope (Olympus) with a fluorescence illuminator/IX2-RFA in the 546 excitation light path (Texas Red). Images were taken at 40x magnification for a total of 10 fields of view per cross-section. Images were analyzed using Image J software, where signal intensity (IntDen) was measured after phospholipid bilayers (cell membrane) thresholds were adjusted for. Signal intensity was interpreted as the IMCL content.

Hematoxylin and Eosin (H&E) Staining for Cross-Sectional Area. Tissue samples from the gastrocnemius were cut at the mid-belly for cross-sectional area (CSA) as previously described. Cross-sections were allowed to air dry at RT for 10-min prior to staining. Hematoxylin staining (Sigma-Aldrich) was performed for 15-mins, followed by Scott's Tap Water Substitute (Sigma-Aldrich) and a final rinse in 18-MΩ H_2O to visualize myonuclei. This was followed immediately with an Eosin stain for 1-min and dehydration in 95% and 100% reagent alcohol (Fisher Scientific), followed by clearing step in Xylene (VWR) for 1-min and mounted with Permount (Fisher Scientific) and cover slipped. Imaging was performed using 10x magnifications to capture the entire cross section and stitched with image composite editor (Microsoft). 500 myofibers were outlined from various regions for CSA using Image J software. Pixels were normalized to 100μm scale bar and total area within each myofiber were compiled and expressed as relative percentage.

Statistical Analysis. Statistical analyses were performed using Graph Pad Prism 6 software. Two-way ANOVA ($SkM^{PKC\theta WT}$/$SkM^{PKC\theta KO}$ x RD/HFD) was performed to

determine whether a significant interaction existed between factors for body/muscle weight, CSA and blood glucose. If a significant interaction was detected, Turkey's *post hoc* comparisons were performed to identify the source of significance with $p<0.05$. Ordinary One-way ANOVA followed by Turkey's multiple comparison tests was used for gene/protein expression relative to GAPDH. One-way ANOVA was used followed by Kruskal-Wallis multiple comparison test for oil red o staining. Grubbs method was used to assess any outliers within data sets at $\alpha=0.05$.

RESULTS

Using the Cre/lox system to generate skeletal muscle specific knock out of PKCθ, we cross-bred female mice of a mixed 129/C57 background homozygous for PKCθ floxed allele with male mice of a FVB/C57 background heterozygous for mutant Myod-iCre. Confirmation of $PKC\theta^{loxP/loxP}$ was performed using primers targeting intron 4 of PKCθ followed by PCR for MyoD1 allele and iCre mutant allele (Figure 1).

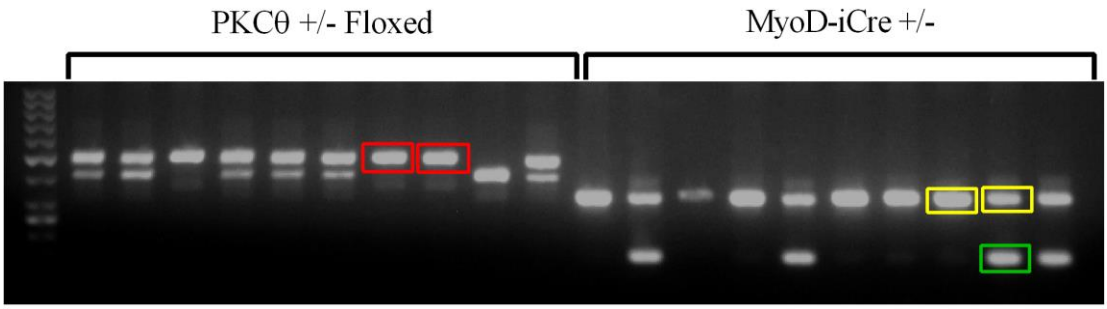

Figure 1: Genotyping for PKCθ floxed allele and MyoD-iCre mutant allele. Mice homozygous for PKCθ floxed allele (459bp, red) were chosen for breeding or 15-wk diet. PKCθ floxed mice were further sub dived into $SkM^{PKC\theta KO}$ groups if heterozygous for MyoD1 allele (343bp, yellow) and iCre mutant allele (149bp, green) and mice homozygous for MyoD1 were used as controls ($SkM^{PKC\theta WT}$).

In total 33 male mice were subjected to 15-wk of either a RD fed chow or HFD fed chow. Upon competition of 15-wk diet, tissue homogenates were analyzed for PKCθ expression via RT-PCR (Figure 2). The analysis of PKC familial isoforms was performed to verify that there was no compensatory upregulation or loss of PKC isoforms due to genetic deletion of PKCθ in skeletal muscle (Figure 2). Protein expression of PKCθ was also reported in both $SkM^{PKC\theta WT}$ and $SkM^{PKC\theta KO}$ gastrocnemius tissue as well as protein lysates of the heart and adipose tissue to verify that the Cre/lox system was

skeletal muscle specific and did not display any “leakiness” in other musculature or neighboring tissues (Figure 3A and 3B).

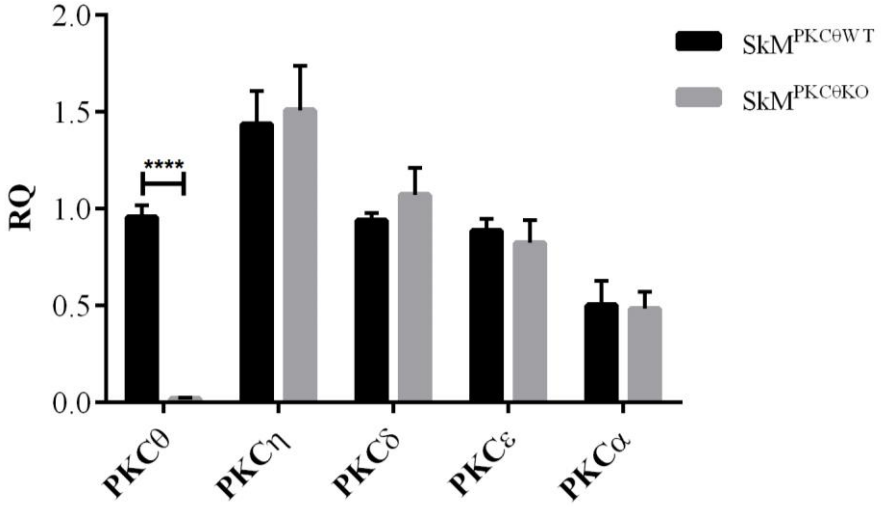

Figure 2: Cre/lox model effectively attenuates mRNA expression of PKCθ in Skeletal muscle without compensatory mechanisms evoked in familial isoforms. Quantification of PKCθ expression in the Plantaris of $SkM^{PKC\theta WT}$; **** $p < 0.0001$ compared to $SkM^{PKC\theta KO}$. $n = 4$ per group/ RT-PCR run. Data expressed as mean relative quantification ± SEM.

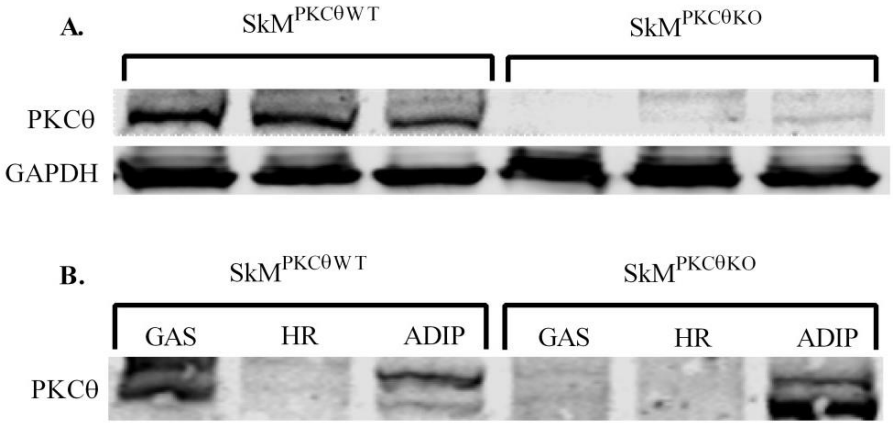

Figure 3: Protein confirmation of PKCθ knock out specific to skeletal muscle of $SkM^{PKC\theta KO}$ mice. (A) $SkM^{PKC\theta WT}$ plantaris observed protein expression of PKCθ relative to GAPDH compared to $SkM^{PKC\theta KO}$ plantaris protein expression; (B) PKCθ protein expression is unaltered in nonspecific tissue of $SkM^{PKC\theta KO}$.

To ensure that there was no developmental defect in our mice due to SkM$^{PKC\theta KO}$, all mice were weighed post-weaning/pre-diet (3-wk). Figure 4 displays no significant discrepancies in pre-diet weights between groups, as any variability seen within or between groups was most likely a consequence of litter sizes (5-13 pups per birth). Body weight was measured weekly, beginning the day of their weaning. Weights were measured every 7-day post for 15-wk. Significant changes in body weight were observable between RD-SkM$^{PKC\theta WT}$ and HFD-SkM$^{PKC\theta WT}$ mice by 7-wk ($p<0.05$) (Figure 5). Significant increases in body weight for HFD- SkM$^{PKC\theta KO}$ mice were apparent by 9-wk ($p<0.05$) compared to RD-SkM$^{PKC\theta KO}$ mice (Figure 5). By 11-wk weight gain in HFD-SkM$^{PKC\theta KO}$ was effectively attenuated ($p<0.05$) compared to HFD-SkM$^{PKC\theta WT}$ controls and differences were maintained through 15-wk (Figure 5).

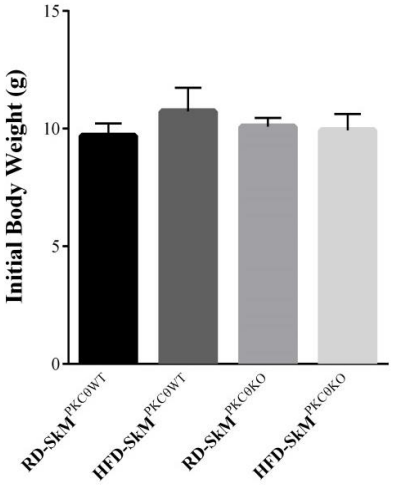

Figure 4: At 3-wk of age male mice were weighed prior to their respective diets. n = 33. Data expressed as mean ± SEM.

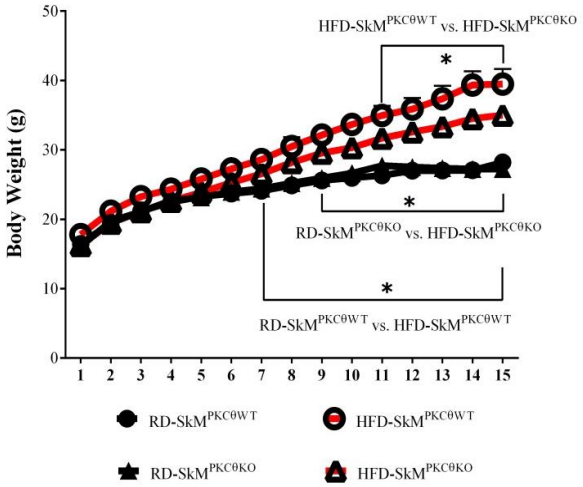

Figure 5: Male mice weights 1xwk for 15-wk. n = 33. Statistical analysis was performed using two-way ANOVA RM by column. Data expressed as means ± SEM.

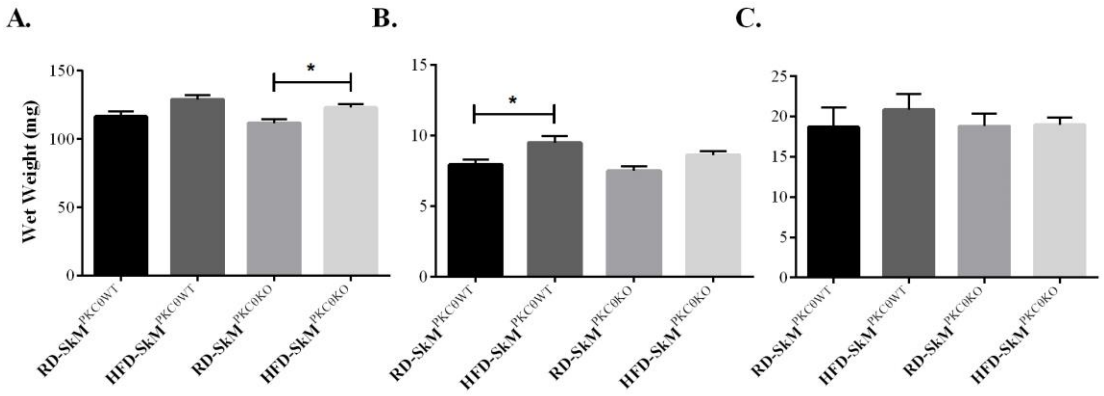

Figure 6: Skeletal muscle wet weight at 18-wk of age. (A) Gastrocnemius wet weight from right hindlimb was greater in HFD-SkM^{PKC0KO} groups; * $p < 0.05$ compared to RD-SkM^{PKC0KO} groups; (B) In the soleus muscle wet was significantly greater in only the HFD-SkM^{PKC0WT} group; * $p < 0.05$ compared to RD-SkM^{PKC0WT} group; (C) No significant differences were observed in the Plantaris. n = 6 to 11 per hindlimb muscle. Data expressed as mean wet weight ± SEM.

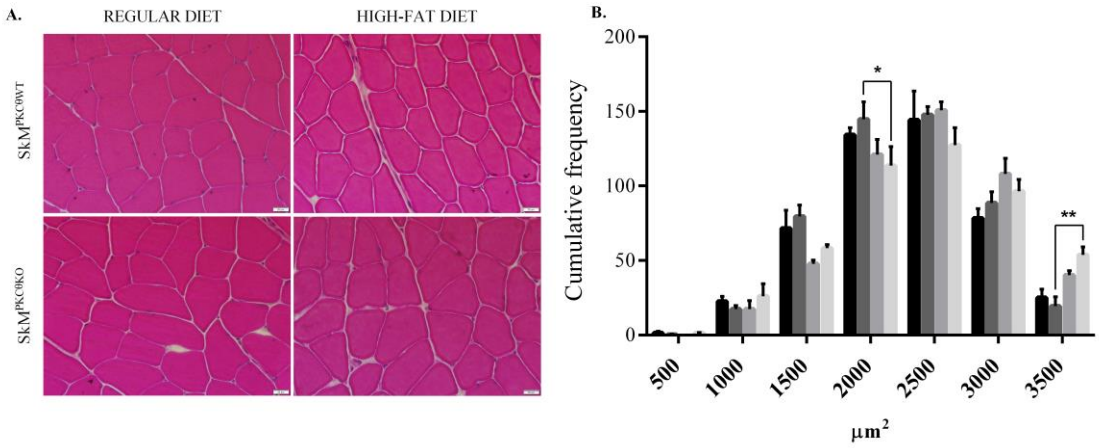

Figure 7**:** H&E stain for CSA of gastroc. (A) 10mm thick cross sections were taken from the mid-belly of the gastrocnemius and imaged under 40x magnification; (B) Myofibers were outlined and area within was quantified using ImageJ with pixels normalized to the scale bar (mm). 500 fibers were measured from each cross section and seperated at 500µm2 intervals. HFD-SkM^{PKC0WT} had significant accumulation of 2000µm^2 fibers; * $p < 0.05$ as well as a decrease in 3000µm^2 fibers; ** $p < 0.01$ compared to HFD-SkM^{PKC0KO}. n = 3 mice from each group. Data expressed as cumulative frequency ± SEM.

Skeletal muscle weights of the gastrocnemius, plantaris and soleus were weighed individually for each mouse at 18-wk of age. Increases in wet weight were only significant in the gastrocnemius of the HFD groups ($p< 0.001$); compared to RD groups, which likely atoned to the increase mechanical loading the gastrocnemius was placed

under from the weight gain (Figure 6). Myofiber CSA was determined using H&E stained cross-sections from the gastrocnemius (Figure 7a).

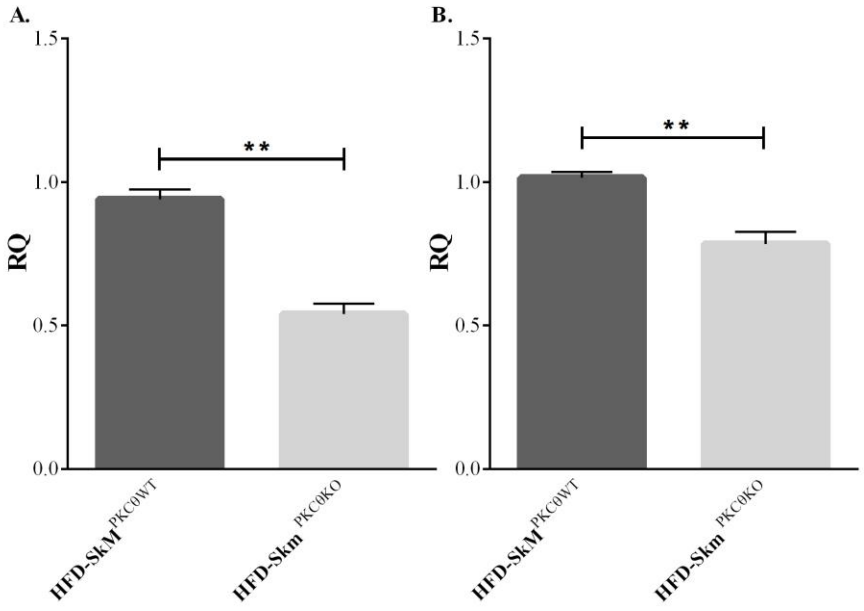

Figure 8**:** Atrogene expression in HFD fed mice. (A) MuRF1 gene expression relative to GAPDH in HFD-SkM$^{PKC\theta WT}$; ** $p < 0.01$ compared to HFD-SkM$^{PKC\theta KO}$; (B) MAFbx gene expression relative to GAPDH in HFD-SkM$^{PKC\theta WT}$; ** $p < 0.01$ compared to HFD-SkM$^{PKC\theta KO}$. *n* = 3. Data expressed as mean relative quantification ± SEM.

.

In the analysis of CSA we did observe considerable discrepancies between HFD cohorts. SkM$^{PKC\theta WT}$ had increased smaller (2000μm^2) myofibers ($p<0.05$) compared to SkM$^{PKC\theta KO}$ (Figure 7b). In line with this finding SkM$^{PKC\theta KO}$ showed an increased frequency of larger (3500μm^2) myofibers ($p<0.01$) compared to SkM$^{PKC\theta WT}$ (Figure 7b). Attempts to investigate the apparent discrepancy in myofiber size between HFD groups showed elevated mRNA expression of muscle specific E3 ubiquitin ligases; Muscle RING finger 1 (MuRF1) and muscle atrophy F-box (MAFbx)/atrogin-1 (Figure 8).

MuRF1 and MAFbx expression in the gastrocnemius of HFD-SkM$^{PKC\theta WT}$ mice were significantly higher ($p<0.01$) compared to HFD-SkM$^{PKC\theta KO}$ mice.

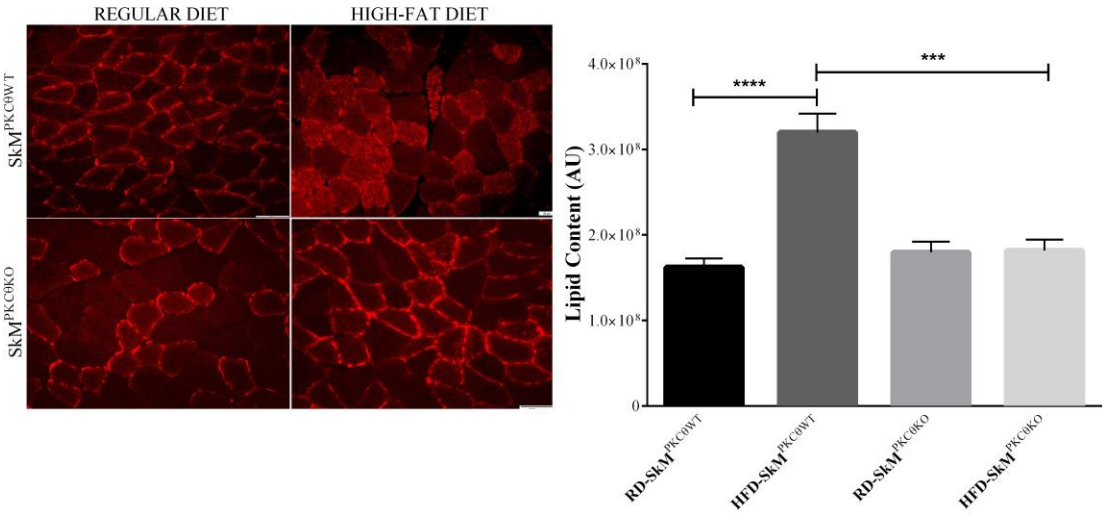

Figure 9: Decreased lipid accumulation in as well as Fatty acid binding protein expression in HFD-SkM$^{PKC\theta KO}$. Quantification of oil red o staining was performed using fluorescent microscopy. HFD-SkM$^{PKC\theta WT}$ demonstrated considerable lipid accumulation; **** $p < 0.0001$ compared to RD-SkM$^{PKC\theta WT}$; HFD-SkM$^{PKC\theta KO}$ demonstrated significant protection from lipid accumulation; *** $p < 0.001$ compared to HFD-SkM$^{PKC\theta WT}$. $n = 4$ per group. Data expressed as mean signal intensity ± SEM.

Metabolic defects due to HFD were assessed in skeletal muscle using oil red o staining. Oil red o's affinity for lipid molecules allows for the fluorescent imaging and quantitative comparison of intracellular staining intensity. The overall intramyocellular staining is noticeably increased in HFD-SkM$^{PKC\theta WT}$ gastrocnemius when viewed alongside both RD groups as well as HFD-SkM$^{PKC\theta KO}$ skeletal muscle (Figure 9). In order to delineate between ectopic and intracellular lipid accumulation, upper thresholds were determined empirically for each field of view. With the use of imageJ, signal intensity was acquired as the IntDen of pixels below the upper threshold with significant elevations of lipid accumulation in the HFD-SkM$^{PKC\theta WT}$ ($p<0.0001$) compared to RD-

SkM$^{PKC\theta WT}$ and ($p<0.001$) compared to HFD-SkM$^{PKC\theta KO}$ mice (Figure 9). No reported significance existed between RD-SkM$^{PKC\theta KO}$ and HFD-SkM$^{PKC\theta KO}$ mice. The increase in IMCL content found in the HFD-SkM$^{PKC\theta KO}$ group was as expected, the attenuated effect in our HFD-SkM$^{PKC\theta KO}$ prompted further investigation into potential metabolic regulators of fatty acid storage.

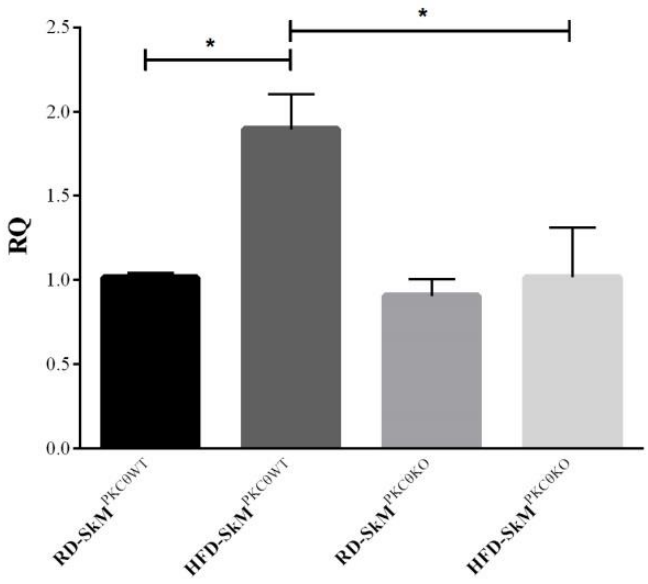

Figure 10: PGC-1α mRNA expression in gastrocnemius. Elevated expression levels of PGC-1α in HFD-SkM$^{PKC\theta WT}$; * $p < 0.05$ compared to RD-SkM$^{PKC\theta WT}$ and HFD-SkM$^{PKC\theta KO}$. n=3. Data is expressed as mean relative quantification of PGC-1α to GAPDH ± SEM.

Peroxisome proliferator-activated receptor gamma coactivator (PGC)-1α gene expression, was demonstrated to be significantly elevated in the gastrocnemius of HFD-SkM$^{PKC\theta WT}$ ($p<0.05$) when compared to RD-SkM$^{PKC\theta WT}$ (Figure 10). HFD-SkM$^{PKC\theta KO}$ mice expression levels of PGC-1α remained unchanged compared to RD groups and were significantly lower ($p<0.05$) than HFD-SkM$^{PKC\theta WT}$ mice (Figure 10).

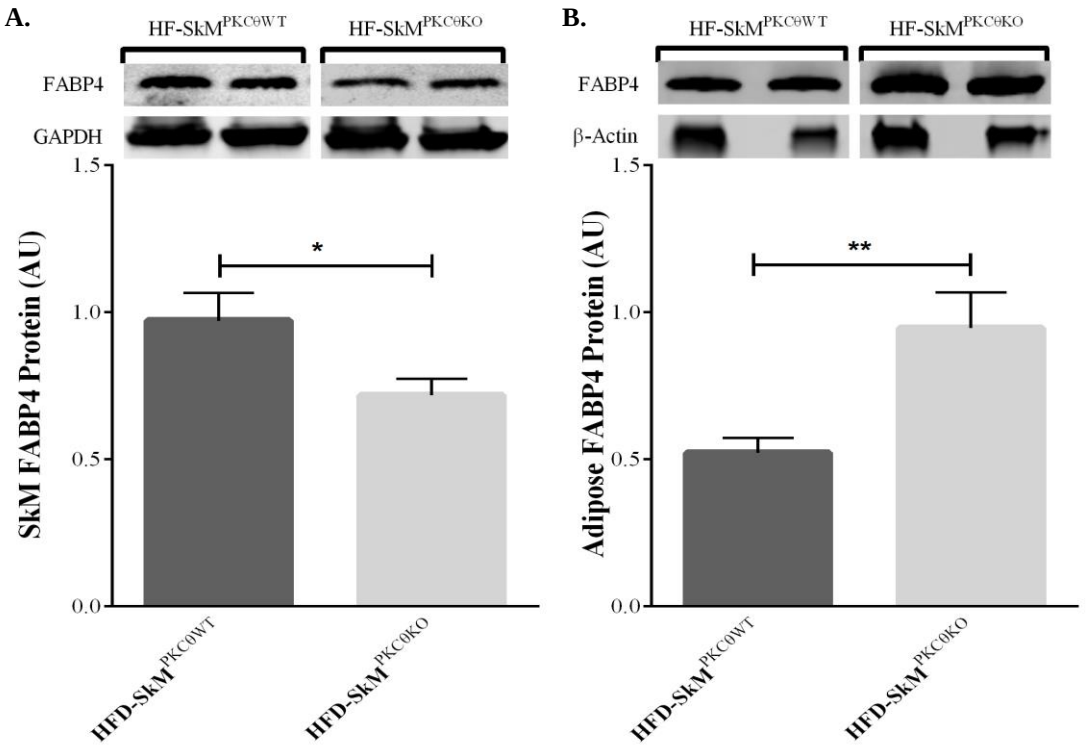

Figure 11: FABP4 expression in Skeletal and adipose tissue. (A) HFD-SkM$^{PKC\theta KO}$ exhibited a reduced protein accumulation of FABP4; * $p < 0.05$ compared to HFD-SkM$^{PKC\theta WT}$. (B) In Adipose tissue, HFD-SkM$^{PKC\theta WT}$ display a decrease in FABP4 expression; ** $p < 0.01$ compared to HFD-SkM$^{PKC\theta KO}$ mice; $n = 5$ for both groups. Data expressed as mean FABP4 signal intensity relative to GAPDH or β-Actin ± SEM.

The analysis of fatty acid binding protein (FABP) 4 content was also demonstrated to be elevated in the soleus of HFD-SkM$^{PKC\theta WT}$ ($p<0.05$) mice compared to HFD-SkM$^{PKC\theta KO}$ mice (Figure 11a). Attempts to quantify FABP4 in adipose tissue demonstrated contrasting expression levels for HFD groups, where by an attenuated accretion of FABP4 was found in HFD-SkM$^{PKC\theta WT}$ ($p<0.05$) compared to HFD-SkM$^{PKC\theta KO}$ (Figure 11b). The effects of lipid accumulation on the microenvironment of skeletal muscle were explored by targeting the mRNA expression levels of tumor necrosis factor (TNF)-α in the gastrocnemius. HFD-SkM$^{PKC\theta KO}$, again displayed a significantly ($p<0.05$) attenuated effect from the HFD-feeding compared to HFD-

SkM$^{PKC\theta WT}$ mice (Figure 12). HFD- SkM$^{PKC\theta WT}$ expression levels were also consistently elevated ($p<0.01$) compared to RD-SkM$^{PKC\theta WT}$ mice (Figure 12).

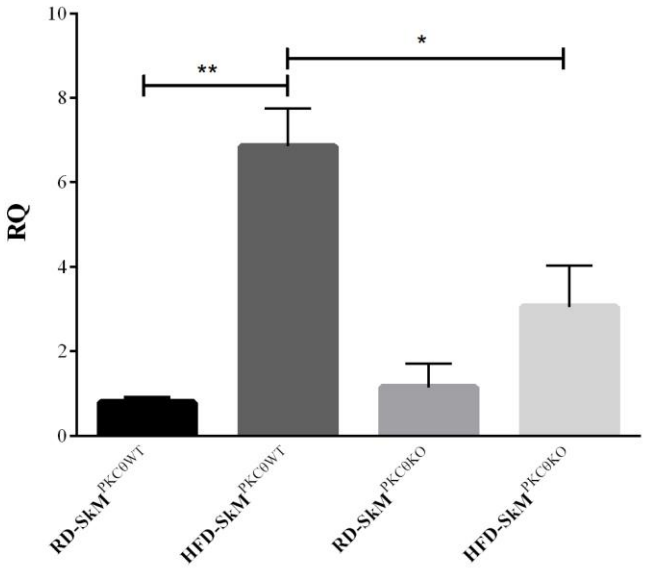

Figure 12: TNF-α expression in gastrocnemius as a marker for diet induced inflammation. HFD-SkM$^{PKC\theta WT}$ display a characteristic of lipid ingestion via an upregulation of TNF-α; ** $p < 0.01$ compared to RD-SkM$^{PKC\theta WT}$. In contrast, HFD-SkM$^{PKC\theta KO}$ exhibit a blunted response to inflammatory gene expression pathways normally associated with HF feeding; * $p < 0.05$ compared to HFD-SkM$^{PKC\theta WT}$. *n* = 3 per group. Data expressed as RQ to GAPDH ± SEM.

Glucose intolerance and subsequent hyperglycemia are well common metabolic defects associated with IR. Upon entering week 12 of their respective diets, fasting blood glucose as well as GTT were employed. Following a 6-hr fast, blood from the tail vein was collected prior to intraperitoneal injection with dextrose. The data collected from fasting blood glucose signified that despite HF-feeding SkM$^{PKC\theta KO}$ mice maintained similar fasted blood glucose levels with matched RD-SkM$^{PKC\theta KO}$. HFD-SkM$^{PKC\theta WT}$ displayed a more common phenotype of elevated fasting blood glucose ($p<0.01$)

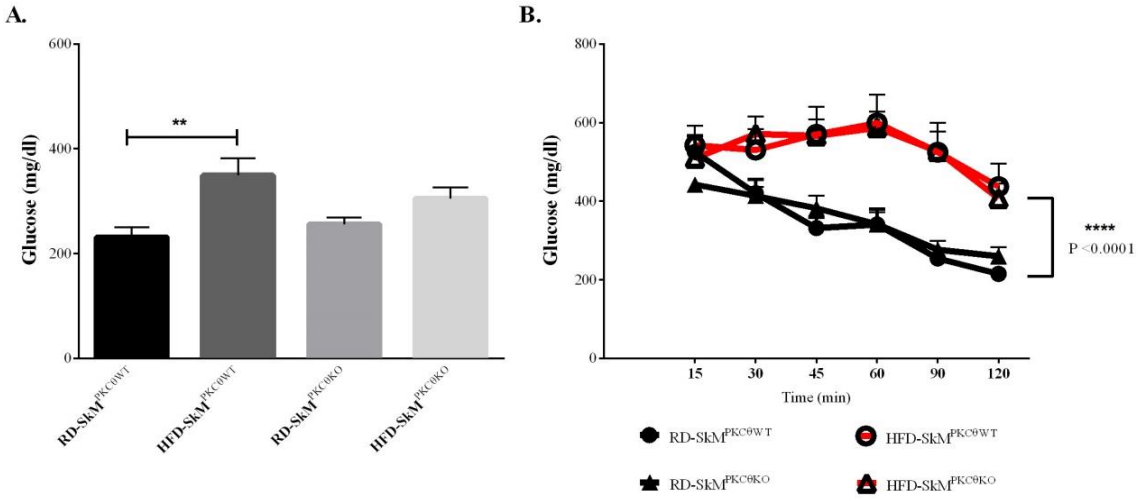

Figure 13: Fasting blood glucose and intraperitoneal glucose tolerance testing. (A) Following a 6-hr fast, tail vein blood samples were measured for glucose content. HFD-SkM$^{PKC\theta WT}$ blood glucose was found to be elevated; ** $p < 0.01$ compared to RD-SkM$^{PKC\theta WT}$; (B) GTT was conducted using 1mg/g body weight over a 2-hr period. Both HFD groups reported similar glucose intolerance; **** $p < 0.0001$ compared to RD groups. *n* = 32. Data expressed as mean blood glucose readings ± SEM.

compared to RD-SkM$^{PKC\theta WT}$ mice (Figure 13a). GTT data presented confounding data despite lowered fasting blood glucose levels and decreased lipid deposition were comparable for genotypes on respective diets. Blood glucose was significantly elevated for both HFD groups starting at the 45-min and continuing through 60, 90, 120-min ($p<0.0001$) compared to RD mice (Figure 13b).

At the conclusion of the 15-wk diet mice were fasted overnight (16-hr) and given an intraperitoneal insulin injection prior to tissue harvesting. Protein extracts of skeletal muscle as well as adipose tissue were analyzed via western blot for phosphorylation of insulin sensitive substrates and known PKCθ insulin inhibitory targets. Initial quantification began with assessing the relative phosphorylation of IRS-1 inhibitory residue ser1101. IP of IRS-1 was performed due to diminished signal of ser1101 phosphorylation. The results of which show no significant attenuation of ser1101 phosphorylation in the absence of PKCθ (Figure 14a). The effects had by a HFD

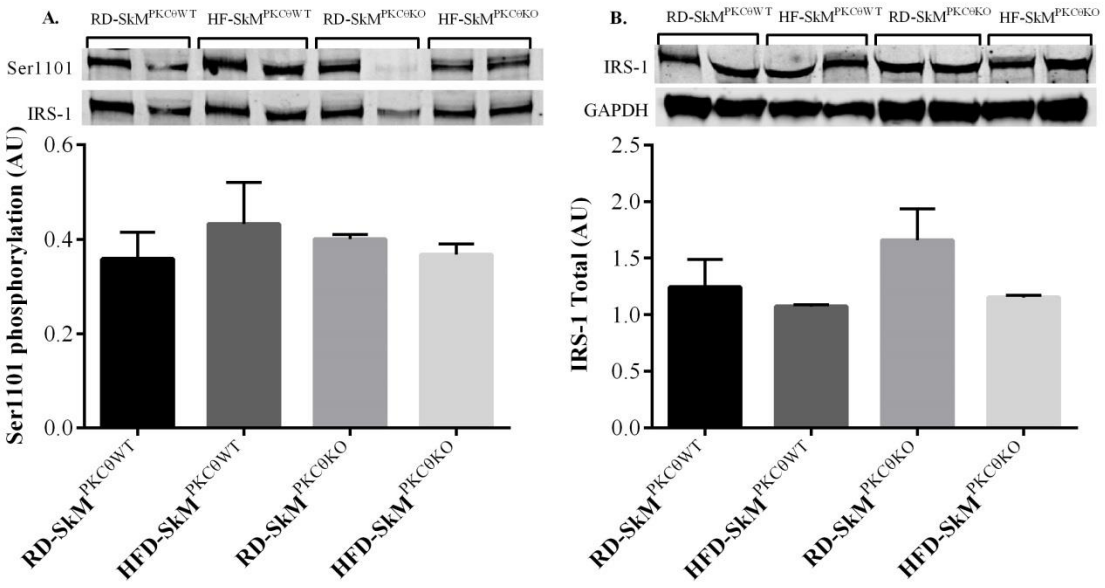

Figure 14: IP protein enrichment of IRS-1 from gastrocnemius. (A) 500mg of protein lysate were used to analyze ser1101 phosphorylation of IRS-1versus IRS-1. *n* = 3 per group. Data expressed as mean signal intensity from IP eluent ± SEM; (B) Western blot was performed with IRS-1 total antibody and normalized to GAPDH. *n* = 3 per group. Data is expressed as relative change as compared to mean RD-SkM$^{PKC\theta WT}$ ± SEM.

on IRS-1 protein concentration were also not significantly altered in either HFD group when compared to RD (Figure 14b).

In order to assess the suppressive effects of PKCθ on insulin sensitive protein kinases downstream of IRS-1 we set out to analyze two key activation sites (Thr308 and Ser473) on Akt. HFD-SkM$^{PKC\theta KO}$ mice had significantly higher phosphorylation of both Akt sites ($p<0.05$) compared HFD-SkM$^{PKC\theta WT}$ mice (Figure 15a and b). Paralleled by a significant decrease in Thr308 phosphorylation in the HFD-SkM$^{PKC\theta WT}$ mice ($p<0.05$) compared to RD-SkM$^{PKC\theta WT}$ mice (Figure 15a). Trends were also observed for Ser473 between groups but did not reach significance ($p=0.088$). In the wake of the significant increase in skeletal muscle insulin sensitivity, we set out to investigate if another insulin sensitive tissue (adipose) had also benefited from said effects. In corroboration with

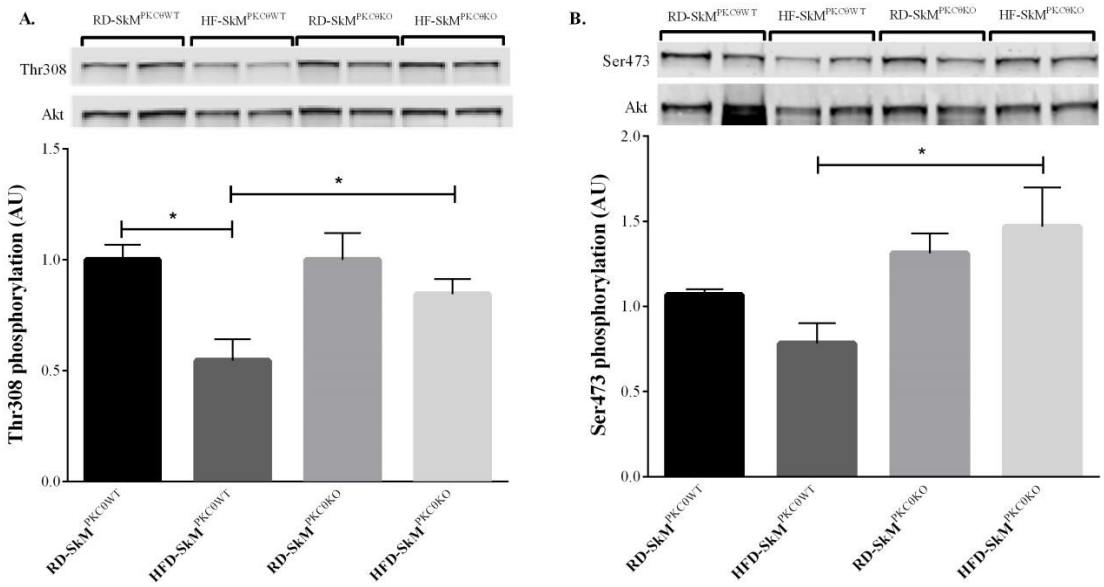

Figure 15: Insulin stimulated phosphorylation of Akt Ser473 and Thr308. (A) Quantification of phospho-site Thr308 of Akt relative to total Akt in gastrocnemius of HFD-SkM$^{PKC\theta WT}$ is attenuated following 15-wk of diet; * $p < 0.05$ compared to RD-SkM$^{PKC\theta WT}$ and HFD-SkM$^{PKC\theta KO}$; (B) Quantification of phospho-site Ser473 of Akt relative to total Akt in gastrocnemius is diminished in HFD-SkM$^{PKC\theta WT}$; * $p < 0.05$ compared to HFD-SkM$^{PKC\theta KO}$. n = 6 per group. Data expressed as mean relative change from RD-SkM$^{PKC\theta WT}$ (pAkt/Akt Total) ± SEM.

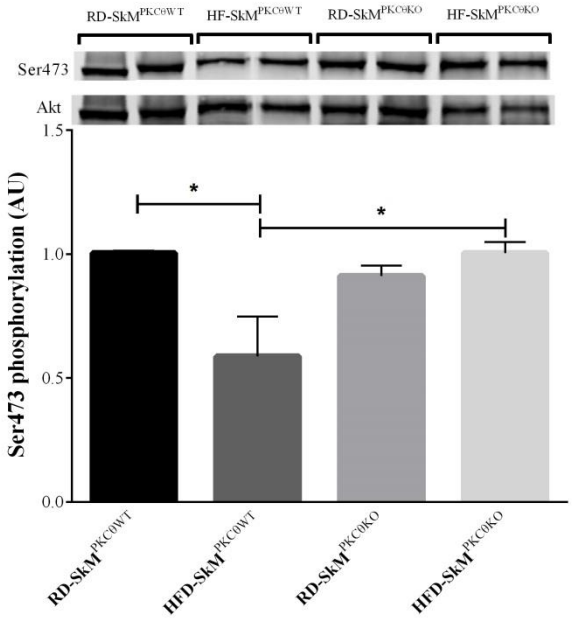

Figure 16: Insulin stimulated Ser473 of Akt in Adipose tissue is attenuated in HFD-SkM$^{PKC\theta WT}$ and unaffected in HFD-SkM$^{PKC\theta KO}$. Phosphorylation of insulin responsive residue Ser473 is decreased in HFD-SkM$^{PKC\theta WT}$; * $p < 0.05$ compared to RD-SkM$^{PKC\theta WT}$ and HFD-SkM$^{PKC\theta KO}$. n = 3 per group. Data expressed as mean relative change compared to RD-SkM$^{PKC\theta WT}$ (Ser473 Akt/Total Akt) ± SEM.

skeletal muscle Akt signaling, we observed an amplified response in the adipose tissue of HFD-SkM$^{PKC\theta WT}$ group for Ser473 ($p<0.05$) compared to the RD-SkM$^{PKC\theta WT}$ group along with a clear absence of an effect on HFD-SkM$^{PKC\theta KO}$ mice ($p<0.05$) compared to HFD-SkM$^{PKC\theta WT}$ mice (Figure 16).

DISCUSSION

Intracellular lipid accumulation and subsequent lipotoxicity evoked from an increase in IMCL storage and spill over are believed by many to be one of the primary causes for IR [10, 17, 22, 49]. Our group has strongly demonstrated that the loss of PKCθ expression specifically from skeletal is protective against HFD-induced skeletal muscle lipid accumulation and insulin resistance. This phenotype is also accompanied by attenuated weight gain and inflammatory/atrophy gene expression. This was accomplished by cross-breeding muscle specific Myod1-iCre mice with a genetically engineered mouse possessing reactive loxP sites flanking intron 4 of PKCθ to produce $SkM^{PKC\theta KO}$ mice. $SkM^{PKC\theta KO}$ was confirmed prior to diet via DNA extract, and post diet completion by way of gene/protein expression. The specificity to skeletal muscle was vital to the success of this study.

Initial attempts using a cardiac/skeletal muscle DN PKCθ KD mouse model lead to IR and elevated body weight by 6 months of age [28]. Interestingly, our $SkM^{PKC\theta KO}$ breeders were regularly aged out to 6-8 months of age and though we did not set out to investigate body weight changes past 18-wk, our group failed to observe any such discrepancies from $SkM^{PKC\theta WT}$ aged matched male breeders (data not presented). Cardiac/Skeletal muscle PKCθ KD mice as well as homozygous PKCθ-null KO mice coincidentally reported similar findings with diet induced IR and obesity. The disparity between our findings and previous reports, attempting to characterize PKCθ's role in IR with diet, point to PKCθ's inclusion or exclusion in non-skeletal muscle tissue, i.e., cardiac, adipose as well its role in satiety and immunity [13, 50, 51]. Of the striated muscle tissues, the heart does not seem to be one of the more abundant accumulation sites

for PKCθ (Figure 3b). Never the less, a recent study did provide considerable evidence that PKCθ KO cardiac myocytes displayed exaggerated apoptotic tendencies in addition to poor overall ventricular function [51]. These data highlight the adverse events that may have gone unnoticed in PKCθ-null mice. Adipose tissue is yet another example of an overlooked site where adverse events may have arisen following PKCθ KO. PKCθ deficient adipocytes would most likely experience enhanced glucose uptake and hypertrophy/hyperplasia, potentially leading to a hastened onset of metabolic dysfunction within adipose tissue and subsequently elevated stress on skeletal muscle [4]. The results attained from of our model can thus be confidently attributed to muscle specific deletion of PKCθ and omits the previous concern or investigation into the confounding variables associated with global KO models.

One potential limitation that may have originated from $SkM^{PKC\theta KO}$ would be the increase stress placed on the liver. Lipid accumulation in the liver enacts its own PKC isoform (Epsilon), which acts similarly to induce IRS-1 inhibition and prevent the suppressive effects of insulin on gluconeogenesis [27]. Chronic elevations in hepatic gluconeogenesis may have resulted in β-cell dysfunction and untimely glucagon secretion by α-cells [27]. All of which may have been masked by the enhanced insulin sensitivity of skeletal muscle. Despite clear discrepancies between IMCL content and intracellular Akt signaling in HFD groups, HF-feeding may have also evoked a competitive inhibition of glycolysis and decreased glucose uptake via the Randle cycle, an effect that may only be apparent when mice were placed under the stress of a GTT [52]. The reduced TNF-α expression, which is likely a consequence of reduced IMCL content, may well be linked to the reduced fasting blood glucose observed in our $SkM^{PKC\theta KO}$ mice. Reduced glut4

expression is often a consequence of increased TNF-α expression along with indicating local M1 macrophage polarization responses to the increase in FFA [49, 53].

The manner in which $SkM^{PKC\theta KO}$ reduced the IMCL content is likely still up for debate and the major underlying contributors have yet to be determined. However, based on our findings a potential theory may exist. Following the quantification of IMCL content, our group began looking at a relatively new and novel player in FFA muscle transport. FABP4 exists as the predominant isoform in adipose tissue; recently it has garnered the distinct activities that have led many to identify FABP4 as an adipocytokine. FABP4's secretion via microvesicles into circulation have been documented to exaggerate β-cell insulin secretion potentially hastening their dysfunction [54]. FABP4 has also been linked to skeletal muscle through its expression in endothelial tissue [55]. A benefit of investigating its protein concentration in adipose tissue is tied directly to the insulin sensitivity of adipose tissue. Insulin inhibits the secretion of FABP4 from adipose tissue which in turn prohibits FABP4's prolonged induction of insulin secretion [54]. HFD-$SkM^{PKC\theta KO}$ mice showed significantly higher concentrations than HFD-$SkM^{PKC\theta WT}$ in adipose tissue following insulin treatment. Increased FABP4 content has been previously witnessed in TGPGC-1α myoblasts [56]. The inherent increase in PGC-1α transcription under sedentary conditions has been reported to be a compensatory mechanism to a HFD, which consequently enhances IMCL content as well as leads to an increase in de novo lipogenesis. The suppression of PGC-1α in our HFD-$SkM^{PKC\theta KO}$ mice may be either a product of reduced adipose lipodystrophy or in some way linked to the maintained intracellular insulin sensitivity, which would promote the use glycolytic pathways for ATP generation over FFA metabolic pathways. This shift in substrate

usage would then theoretically reduce the heavy FFA reliance witnessed in HFD-$SkM^{PKC\theta WT}$ mice back to a more homeostatic mix of glucose and FFA metabolism.

Intramyocellular insulin signaling is dependent upon posttranslational activation of Akt. Full activation is witnessed following the phosphorylation of both Thr308 and Ser473. Although we were unable to distinguish between Akt isoforms, the predominant expression of Akt2 in skeletal muscle limits our concerns as to which downstream pathways were enacted by insulin stimulation. Based on the in vitro work it was not surprising that the effects of $SkM^{PKC\theta KO}$ were more evident with Thr308, as this site is dependent not only on IRS-1/PI3K interactions but also PDK1. PDK1 as mentioned previously along with IRS-1 is a direct target of PKCθ serine phospho-regulation [31]. Thr308 however is also highly implicated in signal transduction pathways involved in myogenesis via mTORC1; however these actions are said to be more in line with Akt1 phosphorylation. Further investigation using techniques to induce muscle hypertrophy while on a HFD may potentially produce a more exaggerated response in CSA between $SkM^{PKC\theta KO}$ mice and $SkM^{PKC\theta WT}$ mice. Findings of decreased Atrogene expression in conjunction with reduced inflammatory gene expression suggest a microenvironment that may overcome the blunted hypertrophy responses previously observed in mice on a HFD [57].

CONCLUSION

Much of the research to date has focused on PKCθ's ability to inhibit skeletal muscle insulin signaling acutely in the presence of lipids [10, 30, 31]. Prior to this research only one group has looked at skeletal muscle insulin signaling on a HFD, but this model ran into some rather confounding results [29]. Based on the work of our lab, we believe the phenotype presented by our $SkM^{PKC\theta KO}$ mice to be one that displays a greater resistance to the deleterious effects of a HFD. This is observed on multiple fronts; 1) reduced/delayed weight gain with a HFD; 2) reduced blood glucose levels; 3) reduced IMCL content in skeletal muscle; 4) reduced levels of TNF-α. All of which suggest immunity to HFD with the deletion of PKCθ in skeletal muscle, further demonstrating that the genetic deletion of $SkM^{PKC\theta KO}$ is a safeguard against the comorbidity related effects of a HFD. $SkM^{PKC\theta KO}$ may also prove to be a useful tool in reversing obesity-driven IR. In combination with diet and/or exercise, IR subjects may exhibit enhanced weight loss and IR reversal. This would in turn help to increase adherence rates to exercise through positive intrinsic reinforcement via meeting their weight loss/blood glucose goals at an accelerated pace. These data should stimulate a renewed research interest in PKCθ with aims toward uncovering all of the potential benefits attributed to $SkM^{PKC\theta KO}$ in reducing the onset and severity of obesity-driven IR.

REFERENCES

1. Ye, J., Mechanisms of insulin resistance in obesity. Front Med, 2013. 7(1): p. 14-24.

2. DeFronzo, R.A. and D. Tripathy, Skeletal muscle insulin resistance is the primary defect in type 2 diabetes. Diabetes Care, 2009. 32 Suppl 2: p. S157-63.

3. Yu, C., et al., Mechanism by which fatty acids inhibit insulin activation of insulin receptor substrate-1 (IRS-1)-associated phosphatidylinositol 3-kinase activity in muscle. J Biol Chem, 2002. 277(52): p. 50230-6.

4. Gao, Z., et al., Inhibition of insulin sensitivity by free fatty acids requires activation of multiple serine kinases in 3T3-L1 adipocytes. Mol Endocrinol, 2004. 18(8): p. 2024-34.

5. Richter, E.A. and N.B. Nielsen, Protein kinase C activity in rat skeletal muscle. Apparent relation to body weight and muscle growth. FEBS Lett, 1991. 289(1): p. 83-5.

6. Baier, G., et al., Molecular cloning and characterization of PKC theta, a novel member of the protein kinase C (PKC) gene family expressed predominantly in hematopoietic cells. J Biol Chem, 1993. 268(7): p. 4997-5004.

7. Osada, S., et al., A new member of the protein kinase C family, nPKC theta, predominantly expressed in skeletal muscle. Mol Cell Biol, 1992. 12(9): p. 3930-8.

8. Griffin, M.E., et al., Free fatty acid-induced insulin resistance is associated with activation of protein kinase C theta and alterations in the insulin signaling cascade. Diabetes, 1999. 48(6): p. 1270-4.

9. Gray, S., et al., Increased skeletal muscle expression of PKC-theta but not PKC-alpha mRNA in type 2 diabetes: inverse relationship with in-vivo insulin sensitivity. Eur J Clin Invest, 2003. 33(11): p. 983-7.

10. Szendroedi, J., et al., Role of diacylglycerol activation of PKCtheta in lipid-induced muscle insulin resistance in humans. Proc Natl Acad Sci U S A, 2014. 111(26): p. 9597-602.

11. Abdul-Ghani, M.A. and R.A. DeFronzo, Pathogenesis of insulin resistance in skeletal muscle. J Biomed Biotechnol, 2010. 2010: p. 476279.

12. Xu, Z.B., et al., Catalytic domain crystal structure of protein kinase C-theta (PKCtheta). J Biol Chem, 2004. 279(48): p. 50401-9.

13. Hage-Sleiman, R., et al., The Novel PKCtheta from Benchtop to Clinic. J Immunol Res, 2015. 2015: p. 348798.

14. Liu, Y., et al., Phosphorylation of the protein kinase C-theta activation loop and hydrophobic motif regulates its kinase activity, but only activation loop phosphorylation is critical to in vivo nuclear-factor-kappaB induction. Biochem J, 2002. 361(Pt 2): p. 255-65.

15. Capel, F., et al., DHA at nutritional doses restores insulin sensitivity in skeletal muscle by preventing lipotoxicity and inflammation. J Nutr Biochem, 2015. 26(9): p. 949-59.

16. Dey, D., et al., Inhibition of insulin receptor gene expression and insulin signaling by fatty acid: interplay of PKC isoforms therein. Cell Physiol Biochem, 2005. 16(4-6): p. 217-28.

17. Dasgupta, S., et al., Mechanism of lipid induced insulin resistance: activated PKCepsilon is a key regulator. Biochim Biophys Acta, 2011. 1812(4): p. 495-506.

18. Li, M., et al., Role of PKCdelta in Insulin Sensitivity and Skeletal Muscle Metabolism. Diabetes, 2015. 64(12): p. 4023-32.

19. Samuel, V.T. and G.I. Shulman, Mechanisms for insulin resistance: common threads and missing links. Cell, 2012. 148(5): p. 852-71.

20. Boyle, J.P., et al., Projection of the year 2050 burden of diabetes in the US adult population: dynamic modeling of incidence, mortality, and prediabetes prevalence. Popul Health Metr, 2010. 8: p. 29.

21. Niu, Y., H. Yuan, and L. Fu, Aerobic exercise's reversal of insulin resistance by activating AMPKalpha-ACC-CPT1 signaling in the skeletal muscle of C57BL/6 mice. Int J Sport Nutr Exerc Metab, 2010. 20(5): p. 370-80.

22. Samuel, V.T. and G.I. Shulman, The pathogenesis of insulin resistance: integrating signaling pathways and substrate flux. J Clin Invest, 2016. 126(1): p. 12-22.

23. Ekkekakis, P., et al., The mysterious case of the public health guideline that is (almost) entirely ignored: call for a research agenda on the causes of the extreme avoidance of physical activity in obesity. Obes Rev, 2016.

24. Coleman, R.A. and D.G. Mashek, Mammalian triacylglycerol metabolism: synthesis, lipolysis, and signaling. Chem Rev, 2011. 111(10): p. 6359-86.

25. Dube, J.J., et al., Exercise-induced alterations in intramyocellular lipids and insulin resistance: the athlete's paradox revisited. Am J Physiol Endocrinol Metab, 2008. 294(5): p. E882-8.

26. Bosma, M., et al., Re-evaluating lipotoxic triggers in skeletal muscle: relating intramyocellular lipid metabolism to insulin sensitivity. Prog Lipid Res, 2012. 51(1): p. 36-49.

27. Shulman, G.I., Ectopic fat in insulin resistance, dyslipidemia, and cardiometabolic disease. N Engl J Med, 2014. 371(12): p. 1131-41.

28. Serra, C., et al., Transgenic mice with dominant negative PKC-theta in skeletal muscle: a new model of insulin resistance and obesity. J Cell Physiol, 2003. 196(1): p. 89-97.

29. Gao, Z., et al., Inactivation of PKCtheta leads to increased susceptibility to obesity and dietary insulin resistance in mice. Am J Physiol Endocrinol Metab, 2007. 292(1): p. E84-91.

30. Kim, J.K., et al., PKC-theta knockout mice are protected from fat-induced insulin resistance. J Clin Invest, 2004. 114(6): p. 823-7.

31. Wang, C., et al., Protein kinase C theta (PKCtheta)-dependent phosphorylation of PDK1 at Ser504 and Ser532 contributes to palmitate-induced insulin resistance. J Biol Chem, 2009. 284(4): p. 2038-44.

32. Li, Y., et al., Protein kinase C Theta inhibits insulin signaling by phosphorylating IRS1 at Ser(1101). J Biol Chem, 2004. 279(44): p. 45304-7.

33. Lemmon, M.A. and J. Schlessinger, Cell signaling by receptor tyrosine kinases. Cell, 2010. 141(7): p. 1117-34.

34. Yuan, M., et al., Reversal of obesity- and diet-induced insulin resistance with salicylates or targeted disruption of Ikkbeta. Science, 2001. 293(5535): p. 1673-7.

35. Cleasby, M.E., et al., Functional studies of Akt isoform specificity in skeletal muscle in vivo; maintained insulin sensitivity despite reduced insulin receptor substrate-1 expression. Mol Endocrinol, 2007. 21(1): p. 215-28.

36. Hoy, A.J., et al., Lipid and insulin infusion-induced skeletal muscle insulin resistance is likely due to metabolic feedback and not changes in IRS-1, Akt, or AS160 phosphorylation. Am J Physiol Endocrinol Metab, 2009. 297(1): p. E67-75.

37. Wang, X., et al., Palmitate induced insulin resistance by PKCtheta-dependent activation of mTOR/S6K pathway in C2C12 myotubes. Exp Clin Endocrinol Diabetes, 2010. 118(9): p. 657-61.

38. Pederson, T.M., D.L. Kramer, and C.M. Rondinone, Serine/threonine phosphorylation of IRS-1 triggers its degradation: possible regulation by tyrosine phosphorylation. Diabetes, 2001. 50(1): p. 24-31.

39. Manna, P. and S.K. Jain, Phosphatidylinositol-3,4,5-triphosphate and cellular signaling: implications for obesity and diabetes. Cell Physiol Biochem, 2015. 35(4): p. 1253-75.

40. Rosen, S.A., et al., Understanding the relative affinity and specificity of the pleckstrin homology domain of protein kinase B for inositol phosphates. Phys Chem Chem Phys, 2012. 14(2): p. 929-36.

41. Ijuin, T. and T. Takenawa, Regulation of insulin signaling by the phosphatidylinositol 3,4,5-triphosphate phosphatase SKIP through the scaffolding function of Pak1. Mol Cell Biol, 2012. 32(17): p. 3570-84.

42. Manning, B.D., Insulin signaling: inositol phosphates get into the Akt. Cell, 2010. 143(6): p. 861-3.

43. Bayascas, J.R., et al., Mutation of the PDK1 PH domain inhibits protein kinase B/Akt, leading to small size and insulin resistance. Mol Cell Biol, 2008. 28(10): p. 3258-72.

44. Karlsson, H.K., et al., Insulin-stimulated phosphorylation of the Akt substrate AS160 is impaired in skeletal muscle of type 2 diabetic subjects. Diabetes, 2005. 54(6): p. 1692-7.

45. Liu, P., et al., PtdIns(3,4,5)P3-Dependent Activation of the mTORC2 Kinase Complex. Cancer Discov, 2015. 5(11): p. 1194-209.

46. Pfeifhofer, C., et al., Protein kinase C theta affects Ca2+ mobilization and NFAT cell activation in primary mouse T cells. J Exp Med, 2003. 197(11): p. 1525-35.

47. Marino, J.S., et al., Suppression of protein kinase C theta contributes to enhanced myogenesis In vitro via IRS1 and ERK1/2 phosphorylation. BMC Cell Biol, 2013. 14(1): p. 39.

48. Koopman, R., G. Schaart, and M.K. Hesselink, Optimisation of oil red O staining permits combination with immunofluorescence and automated quantification of lipids. Histochem Cell Biol, 2001. 116(1): p. 63-8.

49. Varma, V., et al., Muscle inflammatory response and insulin resistance: synergistic interaction between macrophages and fatty acids leads to impaired insulin action. Am J Physiol Endocrinol Metab, 2009. 296(6): p. E1300-10.

50. Park-York, M., et al., PKCtheta expression in the amygdala regulates insulin signaling, food intake and body weight. Obesity (Silver Spring), 2013. 21(4): p. 755-64.

51. Paoletti, R., et al., Protein kinase Ctheta is required for cardiomyocyte survival and cardiac remodeling. Cell Death Dis, 2010. 1: p. e45.

52. Randle, P.J., et al., The glucose fatty-acid cycle. Its role in insulin sensitivity and the metabolic disturbances of diabetes mellitus. Lancet, 1963. 1(7285): p. 785-9.

53. de Alvaro, C., et al., Tumor necrosis factor alpha produces insulin resistance in skeletal muscle by activation of inhibitor kappaB kinase in a p38 MAPK-dependent manner. J Biol Chem, 2004. 279(17): p. 17070-8.

54. Furuhashi, M., et al., Fatty Acid-Binding Protein 4 (FABP4): Pathophysiological Insights and Potent Clinical Biomarker of Metabolic and Cardiovascular Diseases. Clin Med Insights Cardiol, 2014. 8(Suppl 3): p. 23-33.

55. Elmasri, H., et al., Endothelial cell-fatty acid binding protein 4 promotes angiogenesis: role of stem cell factor/c-kit pathway. Angiogenesis, 2012. 15(3): p. 457-68.

56. Mormeneo, E., et al., PGC-1alpha induces mitochondrial and myokine transcriptional programs and lipid droplet and glycogen accumulation in cultured human skeletal muscle cells. PLoS One, 2012. 7(1): p. e29985.

57. Sitnick, M., S.C. Bodine, and J.C. Rutledge, Chronic high fat feeding attenuates load-induced hypertrophy in mice. J Physiol, 2009. 587(Pt 23): p. 5753-65.